Substrate Integrated Waveguide Filters Based on a Dielectric Layer with Periodic Perforations

Lorenzo Silvestri, *Student Member, IEEE*, Enrico Massoni, *Student Member, IEEE*, Cristiano Tomassoni, *Member, IEEE*, Angela Coves, *Member, IEEE*, Maurizio Bozzi, *Senior Member, IEEE*, and Luca Perregrini, *Fellow, IEEE*

Abstract—This paper presents a novel class of substrate integrated waveguide (SIW) filters, based on periodic perforations of the dielectric layer. The perforations allow to reduce the local effective dielectric permittivity, thus creating waveguide sections below cutoff. This effect is exploited to implement immittance inverters through analytical formulas, providing simple design rules for the direct synthesis of the filters. The proposed solution is demonstrated through the design and testing of several filters with different topologies (including half-mode SIW and folded structures). The comparison with classical iris-type SIW filters demonstrates that the proposed filters exhibit better performance in terms of sensitivity to fabrication inaccuracies and rejection bandwidth, at the cost of a slightly larger size.

Index Terms—Filters, resonator filters, substrate integrated waveguide, tolerance analysis.

I. INTRODUCTION

THE SUBSTRATE INTEGRATED WAVEGUIDE (SIW) technology has been the object of intense and ever-growing research activities in the last decade [1], [2]. The SIW technology combines the complete shielding and fairly low losses, with the simple and cost-effective manufacturing, thus representing the ideal platform for the development of the next generation of wireless systems.

Besides the traditional SIW, several novel structures have been proposed, to reduce the size, increase the single-mode bandwidth, and decrease losses. Among them, the folded SIW [3], [4] allows to reduce by half the width of the waveguide (at the cost of a dual-layer manufacturing), the half-mode SIW [5], [6] reduces the width and increases the single-mode bandwidth of a factor two, the slab SIW [7] allows to increase the single-mode bandwidth, the ridge SIW [8], [9] increases the bandwidth and reduces the size (at the cost of a higher
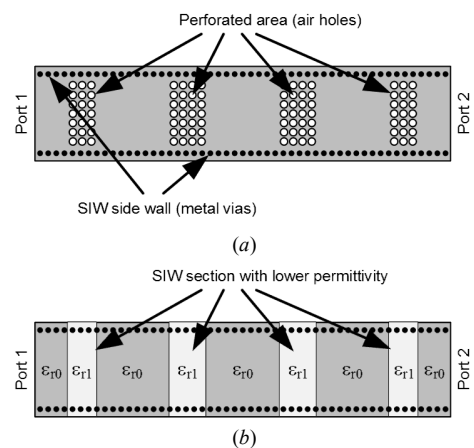
Fig. 1. SIW filter with periodic perforations: (*a*) Physical geometry of the filter; (*b*) Equivalent structure based on the homogeneous permittivity of the perforated area.

fabrication complexity), and the empty SIW [10] cuts dielectric losses and extends the power handling capabilities (at the cost of a slightly larger size).

Similarly, a number of novel SIW filter configurations have been presented to improve filter performance, reduce losses, and minimize the footprint [11]-[13]. Half-mode [14], folded [15], and quarter-mode [16] SIW cavities have been adopted to reduce the filter size, and the substrate integrated coaxial line [17] has been used to obtain wide stopband and compact size. The use of defected ground structures and of extracted poles have been proposed in [18], [19] for improving the out-of-band rejection. Miniature SIW cavities adopting interdigital capacitors [20] have been proposed to reduce filter dimensions. The use of empty surface-mounted waveguide cavities in [21] allows to implement filters with higher quality factor.

Recently, the preliminary investigation of a band-pass filter based on a periodically drilled SIW structure has been proposed [22]: perforations in the dielectric substrate (Fig. 1(*a*)) allow to reduce the local effective permittivity, thus creating waveguide sections below cutoff (Fig. 1(*b*)). Further developments of this class of filters have been reported in two conference papers [23], [24], adding flexibility to the design and extending this concept to half-mode SIW structures.
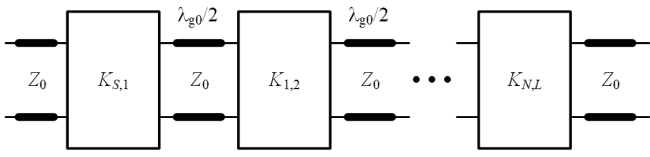
In this paper, a systematic investigation of the properties of

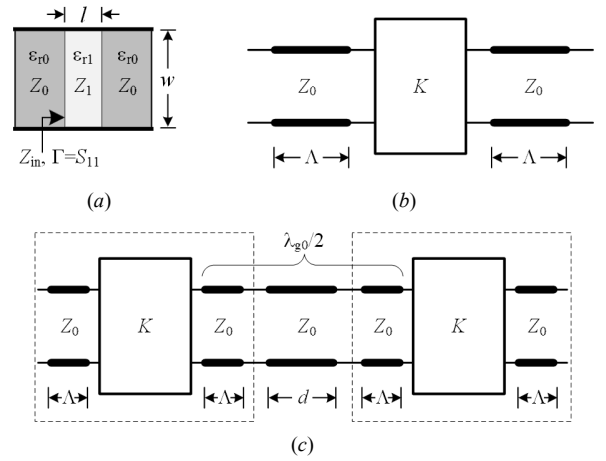Fig. 2. Equivalent circuit of an in-line N-pole filter.

Fig. 3. Evanescent waveguide section: (*a*) Geometry of the evanescent waveguide section; (*b*) Representation as an inverter and two transmission line sections; (*c*) Implementation of a resonator by two inverters.

perforated SIW filters is presented. The waveguide sections with reduced permittivity are exploited to implement immittance inverters. A theoretical study of their properties is reported, along with the guidelines for the fine control of the coupling. Simple models and design rules are presented, and applied to the design of four different pass-band SIW filters, namely a classical SIW filter, a half-mode SIW filter, and two half-mode SIW filters in folded topology (which allows the introduction and control of a transmission zero). An interesting feature of the proposed filter is that the physical length of the resonators is extremely short (about $\lambda_g/6$ in the considered examples), thus allowing relatively compact structures despite of the not so compact coupling elements realized by perforated waveguide sections. It is also demonstrated that these filters exhibit lower sensitivity to fabrication inaccuracies compared to iris-type filters with analogous frequency response. This feature of perforated SIW filters opens the possibility of manufacturing microwave filters by low-cost fabrication technique, such as the punching technique [25].

The paper is organized as follows. Section II presents the operation principle of the filter and the modeling of the immittance inverter based on perforated (evanescent mode) SIW sections. Section III presents the synthesis of a four-pole SIW filter, its fabrication and testing, and the assessment of its low sensitivity to fabrication tolerances. Section IV reports the design and testing of a four-pole filter in half-mode SIW topology, to reduce the dimensions. Finally, Section V shows two prototypes of three-pole half-mode SIW filters in folded configuration, which allow the introduction and control of transmission zeros.

II. OPERATION PRINCIPLE OF THE FILTER

The equivalent circuit of the filtering structure in Fig. 1 can be obtained by modeling the evanescent waveguide sections as impedance inverters (plus two transmission lines), and the propagating waveguide sections connecting two evanescent sections as dispersive transmission lines (Fig. 2).

The normalized impedance inverter $K_{i,j}^{(\mathrm{Nor})} = K_{i,j}/Z_0$ can be evaluated directly from the coupling matrix elements

$$K_{S,1}^{(\mathrm{Nor})} = M_{S,1}\sqrt{\frac{\pi}{2}FBW_{\lambda_g}} \tag{1}$$

$$K_{N,L}^{(\mathrm{Nor})} = M_{N,L}\sqrt{\frac{\pi}{2}FBW_{\lambda_g}} \tag{2}$$

$$K_{i,j}^{(\mathrm{Nor})} = M_{i,j}\frac{\pi}{2}FBW_{\lambda_g} \tag{3}$$

where the subscripts S and L stand for source and load, while indices i and j refer to the i-th and j-th resonator, respectively, and N is the total number of resonators. The fractional bandwidth FBW is calculated by using the waveguide wavelength to account for dispersion

$$FBW_{\lambda_g} = \frac{\lambda_{g2} - \lambda_{g1}}{\lambda_{g0}} \tag{4}$$

being λ_{g1} and λ_{g2} the waveguide wavelengths at the lower and higher pass-band edge, respectively, while λ_{g0} is the waveguide wavelength at the central frequency:

$$\lambda_{g0} = \sqrt{\lambda_{g1}\lambda_{g2}} \tag{5}$$

A. Synthesis of the immittance inverter

The section with reduced permittivity ε_{r1} (Fig. 3(*a*)) acts as an immittance inverter with two transmission line sections (Fig. 3(*b*)). This equivalence is shown by evaluating the reflection coefficient of the evanescent waveguide section.

The propagation constant β_0 of the input and output waveguides is real, whereas the one of the evanescent waveguide β_1 is purely imaginary

$$\beta_0 = \sqrt{\left(\frac{2\pi}{\lambda}\right)^2 \varepsilon_{r0} - \left(\frac{\pi}{w}\right)^2} \tag{6}$$

$$\beta_1 = -j\gamma_1 = \sqrt{\left(\frac{2\pi}{\lambda}\right)^2 \varepsilon_{r1} - \left(\frac{\pi}{w}\right)^2} \tag{7}$$

where λ is the wavelength in vacuum and w is the waveguide width. Analogously, the characteristic impedance Z_0 (in the propagating waveguide section) is real, whereas Z_1 (in the evanescent waveguide section) is imaginary

$$Z_0 = \frac{\omega\mu}{\beta_0} \tag{8}$$

$$Z_1 = \frac{\omega\mu}{\beta_1} = \frac{\omega\mu}{-j\gamma_1} \qquad (9)$$

The input impedance Z_{in} can be expressed as

$$Z_{in} = Z_1 \frac{Z_0 + jZ_1 \tan(\beta_1 l)}{Z_1 + jZ_0 \tan(\beta_1 l)} \qquad (10)$$

where l is the length of the evanescent waveguide section. This allows the evaluation of the reflection coefficient Γ

$$
\begin{aligned}
\Gamma = S_{11} = \frac{Z_{in} - Z_0}{Z_{in} + Z_0} &= \frac{Z_1 \frac{Z_0 + jZ_1 \tan(\beta_1 l)}{Z_1 + jZ_0 \tan(\beta_1 l)} - Z_0}{Z_1 \frac{Z_0 + jZ_1 \tan(\beta_1 l)}{Z_1 + jZ_0 \tan(\beta_1 l)} + Z_0} = \\
&= \frac{j\left(Z_1^2 - Z_0^2\right)\tan(\beta_1 l)}{2Z_0 Z_1 + j\left(Z_1^2 + Z_0^2\right)\tan(\beta_1 l)} = \\
&= -\frac{\left(\gamma_1^2 + \beta_0^2\right)\tanh(\gamma_1 l)}{2 j\gamma_1\beta_0 + \left(\gamma_1^2 - \beta_0^2\right)\tanh(\gamma_1 l)} = \\
&= -\frac{\left(\gamma_1^2 + \beta_0^2\right)\tanh(\gamma_1 l)}{\sqrt{4(\gamma_1\beta_0)^2 + \left(\gamma_1^2 - \beta_0^2\right)^2 \tanh^2(\gamma_1 l)}} \times \\
&\quad e^{-j \arctan\left(\frac{2\gamma_1\beta_0}{\left(\gamma_1^2 - \beta_0^2\right)\tanh(\gamma_1 l)}\right)}
\end{aligned}
\qquad (11)
$$

Therefore, with reference to the Appendix, the evanescent waveguide section can be represented by an impedance inverter and two transmission line sections, as shown in Fig. 3(b). In fact, the normalized inverter of value

$$K^{(Nor)} = \frac{K}{Z_0} = \sqrt{\frac{1 + S_{11}^{(Ampl)}}{1 - S_{11}^{(Ampl)}}} \qquad (12)$$

with

$$S_{11}^{(Ampl)} = -\frac{\left(\gamma_1^2 + \beta_0^2\right)\tanh(\gamma_1 l)}{\sqrt{4(\gamma_1\beta_0)^2 + \left(\gamma_1^2 - \beta_0^2\right)^2 \tanh^2(\gamma_1 l)}} \qquad (13)$$

accounts for the return loss amplitude of the evanescent waveguide section, while the transmission line sections at the inverter ports with length

$$\Lambda = \frac{1}{2\beta_0} \arctan\left(\frac{2\gamma_1\beta_0}{\left(\gamma_1^2 - \beta_0^2\right)\tanh(\gamma_1 l)}\right) \qquad (14)$$

take into account the return loss phase.

In conclusion, (12) and (14) provide analytical formulas for the design of the impedance inverter in Fig. 3(b).
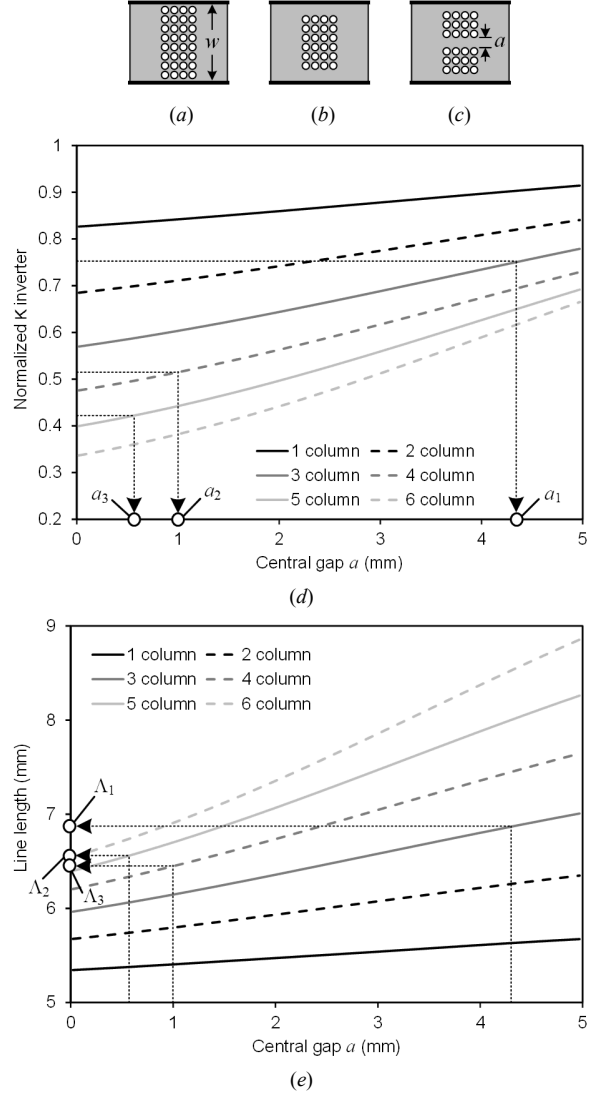

Fig. 4. Model of the evanescent waveguide section: (a), (b), (c) Three different configurations of the perforated evanescent waveguide section; (d) Normalized impedance inverter values $K^{(Nor)}$ versus the central gap a ($w = 16.8$ mm, $\varepsilon_r = 10$, radius of the holes $r = 0.85$ mm, and distance between adjacent holes $\Delta = 0.25$ mm); (e) Line length Λ versus the central gap a.

B. Implementation of the Evanescent Mode Section

The evanescent waveguide section can be obtained by exploiting perforations in the substrate to reduce the dielectric constant, as shown in Fig. 4(a). The perforated substrate exhibits an effective dielectric permittivity ε_{eff}, which assumes an intermediate value between the permittivity of the substrate and of the air [22]. The effective permittivity ε_{eff} is computed as the dielectric permittivity of the homogeneous SIW structure with the same cutoff frequency of the fundamental mode.

With reference to Fig. 4(a), the desired impedance inverter value can be obtained by applying (11) and considering $\varepsilon_{r1} = \varepsilon_{eff}$. As an example, considering a waveguide width of

TABLE I
IMPEDANCE INVERTER ASSOCIATED TO PERFORATED
EVANESCENT WAVEGUIDE LENGTHS (IN MILLIMETERS)

Number of hole columns	Normalized K-inverter		Transmission line length Λ	
	Full-wave (HFSS)	Equation (ε_{eff}=5)	Full-wave (HFSS)	Equation (ε_{eff}=5)
1	0.8231	0.8467	5.332	5.552
2	0.6791	0.7000	5.648	5.864
3	0.5622	0.5814	5.923	6.139
4	0.4673	0.4843	6.150	6.368
5	0.3901	0.4049	6.330	6.551
6	0.3268	0.3398	6.468	6.693

$w=16.8$ mm, a dielectric constant $\varepsilon_r=10$, and holes with radius of $r=0.85$ mm and a side-by-side distance of $\Delta=0.25$ mm, the effective dielectric constant is $\varepsilon_{eff}=5$. Considering this effective dielectric constant and using (12) and (14), an estimation of the equivalent K-inverter and of the transmission line lengths Λ can be found (Fig. 3(b)). The lengths of the evanescent perforated waveguide sections considered in (12) and (14) are related to the number of hole columns (1.7 mm, 3.65 mm, 5.6 mm, 7.55 mm, 9.5 mm, 11.45 mm). In Table I, such results are compared to simulations from the full-wave solver Ansys High Frequency Structural Simulator (HFSS), showing a good agreement.

The limitation of such a structure is that the length of the evanescent waveguide section depends on the number of hole columns, and only discrete values are possible. Instead, the filter design requires a more accurate selection of K-inverter values. To overcome this problem, the structure in Fig. 4(b), obtained by removing the top and bottom hole rows, is adopted. Note that this removal slightly changes the K-inverter value, as removed holes are those positioned where the field is weaker. However, it creates enough space to shift the holes, increasing the gap a between the central hole rows (Fig. 4(c)).

The idea is to use the number of hole columns for a coarse selection of the K-inverter (by using the analytical formulas) and then refine the value by selecting the proper gap a (by using full-wave simulations). This concept is illustrated in Fig. 4(d), where the K-inverter values related to perforated evanescent waveguide sections having a number of hole columns ranging from 1 to 6 are plotted as a function of the gap a. Note that, exploiting the further degree of freedom of the gap a, all possible K-inverter values in the range from 0.34 to 0.91 are attainable. Values lower than 0.34 can be easily obtained by using more than 6 hole columns, while to obtain values larger than 0.91 it is necessary to vary the geometry by reducing the hole radius or increasing the distance between adjacent holes. Finally, in Fig. 4(e) the diagram for the evaluation of the transmission line lengths Λ to be added to the K-inverter ports is shown. The results of Fig. 4(d) and Fig. 4(e) have been obtained from the full-wave solver Ansys HFSS.

A wide range of coupling coefficients can be achieved by changing the number of hole columns and the central gap a. This allows to design filters with large or narrow passband.
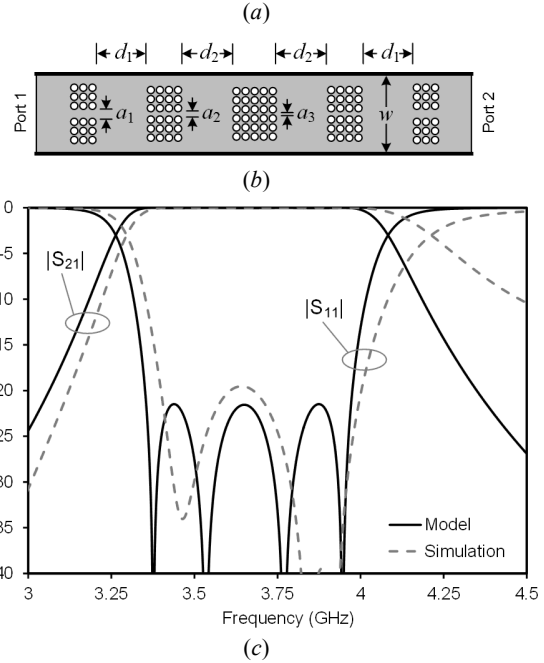

Fig. 5. Synthesis of the four-pole filter with perforations: (a) Coupling matrix of the filter obtained from the synthesis; (b) Geometry of the filter (dimensions in mm: d_1=7.15, d_2=7.44, a_1=4.32, a_2=1, a_3=0.63, and w=16.8); (c) Scattering parameters (results from the synthesis are compared with the HFSS simulation).

In particular, narrow band filters require small coupling, which can be obtained by increasing the length of the waveguide sections below cutoff (i.e., the number of hole columns).

III. FILTER BASED ON PERFORATED SIW

A. Preliminary Synthesis of the Filter

As an example, the design of an in-line filter centered at f_0=3.65 GHz with a fractional bandwidth of FBW=0.16, described by the coupling matrix shown in Fig. 5(a) is here considered.

The first step is the evaluation of the normalized K-inverters by using (1)-(3), thus obtaining $K_{S,1}^{(Nor)} = K_{4,L}^{(Nor)} = 0.75$, $K_{1,2}^{(Nor)} = K_{3,4}^{(Nor)} = 0.515$, $K_{2,3}^{(Nor)} = 0.425$.

The design procedure consists in the use of (12)-(14) to find the lengths l of the evanescent waveguide sections by using the effective dielectric constant of the perforated waveguide (in this case ε_{eff}=5). The resulting lengths are l_1=2.9 mm, l_2=6.9 mm and l_3=9.0 mm. Such lengths can be approximated by a number of hole columns equal to 2, 4 and 5, respectively. This corresponds, for the structure of Fig. 4(b), to normalized K-inverters of value 0.69, 0.48, and 0.41, respectively.

Fine tuned K-inverter values are then obtained by a proper selection of the gap a, with the help of a full-wave simulator. Note that the starting value of the K-inverters should be lower than the desired one, as gap a only allows the increase of this value. This means that the distances l_1, l_2, and l_3 should be rounded to the higher integer.

A faster design procedure is possible by exploiting the diagram of Fig. 4(d), to directly find the number of hole columns and the gap a. Note that the same value of K-inverter can be obtained by using different hole column numbers. As an example, the K-inverter value 0.75 can be obtained by using 2 or 3 columns, the value 0.515 with 4, 5 or 6 columns, while the value 0.425 with 5 or 6 columns. In this example, K_{S1} has been realized by using 3 columns and $a_1=a_5=4.32$ mm, K_{12} by using 4 columns and $a_2=a_4=1$ mm, K_{23} by using 4 columns and $a_3=0.63$ mm. By using the diagram of Fig. 4(e) it is possible to find the length of the transmission lines to be added to the K-inverter: $\Lambda_1=6.87$ mm, $\Lambda_2=6.45$ mm, and $\Lambda_3=6.58$ mm. Such lengths are then subtracted from the resonator ($\lambda_g/2=20.47$ mm), leading to a physical resonator of length $d_1=d_4=20.47-6.87-6.45=7.15$ mm and $d_2=d_3=20.47-6.45-6.58=7.44$ mm (Fig. 5(b)).

In Fig. 5(c), the scattering parameters of the designed filter are compared to the coupling matrix response, showing a very good agreement even though the filter was not optimized.

An interesting feature of this structure is the reduced physical length of the resonators. In fact, while the length of the transmission lines in Fig. 2 is $\lambda_g/2$, the length of the resonator in the physical structure is significantly reduced, resulting in about $\lambda_g/6$ in this example. This reduction, according to Fig. 3(c), is due to the presence of the transmission line sections in the impedance inverter representing the evanescent waveguide sections. This phenomenon also happens in other filtering structures, such as in iris filters, but the resonator length reduction is very limited in those cases. As discussed in Section II, narrower band filters require longer evanescent waveguide sections, thus increasing the size of the filter.

B. Manufacturing and Experimental Validation

Based on the results of the filter synthesis discussed in the previous subsection, the final geometry of the prototype has been obtained. First of all, the equivalent rectangular waveguide adopted in the synthesis has been replaced by the SIW structure [26], using metal vias with a diameter of $d=1$ mm and longitudinal spacing of $s=1.5$ mm to avoid radiation leakage [2]. Moreover, tapered transitions have been added to connect the SIW structure to the input and output microstrip lines, required for measurement purposes. A light full-wave optimization (based on the commercial electromagnetic solver HFSS) was adopted to achieve the final coupling matrix (Fig. 6(a)) and geometrical dimensions of the filter (Fig. 6(b)).

The filter has been fabricated by using a dielectric substrate Taconic CER-10, with a thickness of 0.64 mm, relative dielectric permittivity of $\varepsilon_r=10.0$, loss tangent $\tan\delta=0.0035$,

and metal conductivity $\sigma=5.8\cdot10^7$ S/m. An LPKF E33 milling machine was adopted to pattern the metal layers and to drill the holes through the substrate, and conductive paste was used to metalize the via holes of the side walls. A picture of the prototype is shown in Fig. 6(c). The air holes have been closed by copper tape on both sides (not shown in the picture), to avoid any radiation leakage. A more standard manufacturing process could be the one adopted in [10], based on multilayered printed-circuit board technology.
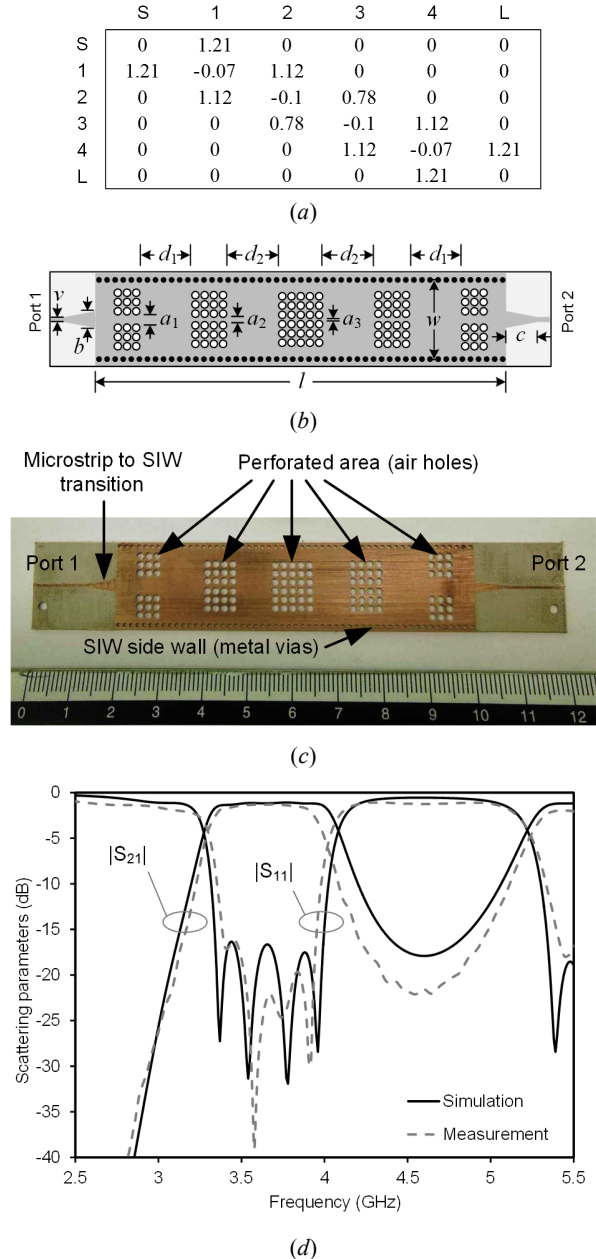
	S	1	2	3	4	L
S	0	1.21	0	0	0	0
1	1.21	-0.07	1.12	0	0	0
2	0	1.12	-0.1	0.78	0	0
3	0	0	0.78	-0.1	1.12	0
4	0	0	0	1.12	-0.07	1.21
L	0	0	0	0	1.21	0

(a)

(b)

(c)

(d)

Fig. 6. Prototype of the four-pole filter based on perforated SIW structure: (a) Coupling matrix of the optimized filter; (b) Geometry of the filter (dimensions in mm: $v=0.6$, $b=2.6$, $d_1=10$, $d_2=7.95$, $a_1=4$, $a_2=0.55$, $a_3=0.25$, $w=17.8$, $c=7$, and $l=81$); (c) Photograph of the prototype; (d) Scattering parameters of the four-pole filter (HFSS simulation compared with measured data).
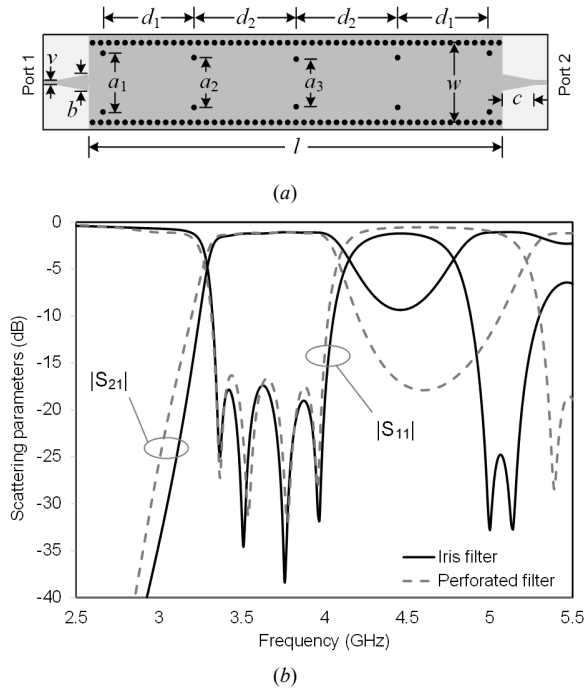
(a)

(b)

Fig. 7. Performance comparison between the perforated SIW filter and a classical iris-type SIW filter: (a) Geometry of the iris-type SIW filter (dimensions in mm: v=0.6, b=3.03, d_1=15.25, d_2=15.1, a_1=13.3, a_2=12.1, a_3=11.4, w=17.425, c=9.5, and l=62.7); (b) Scattering parameters of the perforated SIW filter and the iris-type SIW filter (HFSS simulation).
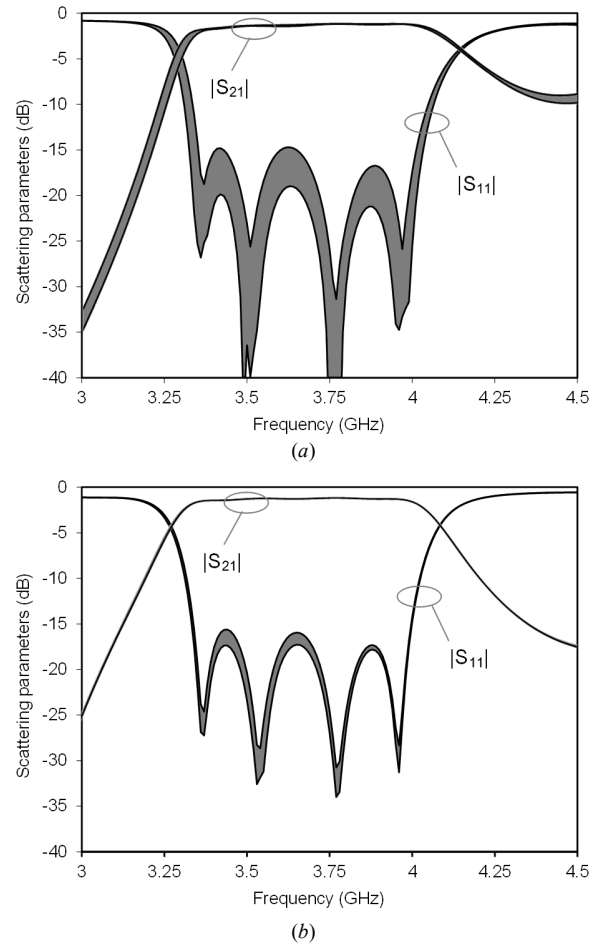

(a)

(b)

Fig. 8. Sensitivity analysis of the iris-type SIW filter and the perforated SIW filter: (a) Spread of the scattering parameters of the iris-type SIW filter; (b) Spread of the scattering parameters of the perforated SIW filter (HFSS simulation).

The prototype has been experimentally characterized: measurements were performed in the frequency band from 2.5 GHz to 5.5 GHz by using an Anritsu Universal Test Fixtures (UTF) 3680 and an Anritsu 37347C vector network analyzer (VNA). No de-embedding was applied to the measured results, to remove the connectors and transitions effect. The comparison between HFSS simulations and the measurements is shown in Fig. 6(d). The small discrepancy is attributed to the combined effect of dielectric permittivity variation and of fabrication inaccuracies (e.g., in the top/bottom metal plates). As a consequence, there is a small shift in the measured position of the filter poles: this determines a slightly narrower pass bandwidth of the filter and a higher out-of-band rejection in the measurement than in the simulation.

The bandwidth, defined at 10 dB input matching, is 630 MHz in the measurement and 660 MHz in the simulation. The measured insertion loss is 1.31 dB at the central frequency f_0=3.65 GHz, compared to 1.15 dB in the simulation.

The simulation allows to investigate the different contribution of losses. Each transition contributes with a loss of 0.19 dB, whereas the SIW filter loss is 0.77 dB, attributed to the dielectric loss (0.47 dB), and to the conductor loss (0.30 dB). There is practically no radiation loss in the filter (0 dB). The size of the circuit is $l \times w$=1442 mm^2.

C. Comparison with Equivalent Inductive Iris Filter

To assess the advantages of the proposed structure, the perforated filter of Fig. 6 is compared with an inductive iris filter, with similar filtering characteristics (same central frequency f_0, number of poles, pass bandwidth, and input matching level), realized on the same dielectric substrate.

The iris-type filter was optimized by using HFSS, and the final geometry is shown in Fig. 7(a). The simulation results of the iris-type filter and of the perforated filter of Fig. 6 are compared in Fig. 7(b). While the insertion loss in the passband is almost identical for the two filters (1.19 dB in the iris-type SIW filter and 1.15 dB in the perforated filter), the perforated filter exhibits a better performance in the out-of-band rejection (with the spurious band appearing at $1.45f_0$=5.22 GHz in the perforated filter and at $1.32f_0$=4.77 GHz in the iris filter). In terms of dimension, the footprint area of the iris filter is 24% smaller than the perforated filter (1091 mm^2 compared with 1442 mm^2).

The perforated filter exhibits outstanding performance over the iris filter in terms of tolerance to fabrication inaccuracies. To investigate the filter tolerance, a Montecarlo analysis was performed by running 2000 HFSS simulations. The position of all the iris posts was changed independently, with a maximum displacement of 50 μm. Analogously, in the perforated filter,

IV. Filter Based on Perforated Half-Mode SIW

The same filter concept was applied to the half-mode SIW structure, with the aim to reduce the size of the filter. The half-mode SIW filter is obtained by removing half of the top metal layer, with a subsequent HFSS re-optimization. The geometry of the filter and the final dimensions are shown in Fig. 10(a).

A prototype has been fabricated by milling machining, using the same manufacturing process described in the previous section, and a picture of the top layer is shown in Fig. 10(b).

The comparison of simulated and measured scattering parameters is reported in Fig. 10(c), in the frequency band from 2.5 GHz to 5.5 GHz. The filter bandwidth, defined at 10 dB input matching, is 730 MHz in the simulation and 760 MHz in the measurement. The insertion loss at the central frequency f_0=3.65 GHz is 2.40 dB in the simulation and 2.15 dB in the measurement. Also in this case, the different contribution of losses have been investigated through simulations. Each transition contributes with a loss of 0.48 dB, whereas the SIW filter loss is 1.44 dB, which is attributed to dielectric loss (0.38 dB), conductor loss (0.43 dB), and to radiation loss (0.63 dB). The size of the circuit is significantly reduced to the case of the filter in Fig. 6, being the footprint area $l \times w$=690 mm^2.

The frequency response of the filter, reported in Fig. 10(c), shows that the insertion loss is larger in the lower portion of the pass band, both in measured and simulated results. To provide a physical insight of this phenomenon, a modal analysis has been performed. In fact, the filter structure can be considered as a cavity resonator, supporting four resonant modes in the pass band of the filter.

The mode spectrum was calculated by using the eigenvalue solver of HFSS. The eigenvalue analysis has been performed under two different boundary conditions of the air box surrounding the cavity: with perfect electric wall boundary condition (where losses depend on dielectric loss and finite metal conductivity, but there is no radiation), and with radiation condition (where also radiation leakage is considered). The electric field amplitude of the four modes is practically unchanged in the two cases, and it is plotted in Fig. 11.

In Table II, the resonance frequencies and the quality factors of the modes are reported, for two cases: in the first case, only conductor and dielectric losses are considered (no radiation), whereas in the second case all sources of loss (conductor, dielectric, and radiation) are taken into account. The resonance frequencies of the four modes exhibit a very limited variation between the two cases, and practically coincide with the four poles of the frequency response of the filter (Fig. 10(c)).

Conversely, the quality factors are significantly affected by radiation: in particular, the first mode reduces its quality factor from 187 to 61. The physical explanation of this effect can be found in the field distribution along the open boundary of the half-mode SIW: in the first mode, the electric field exhibits a uniform phase, thus leading to a non-negligible radiation
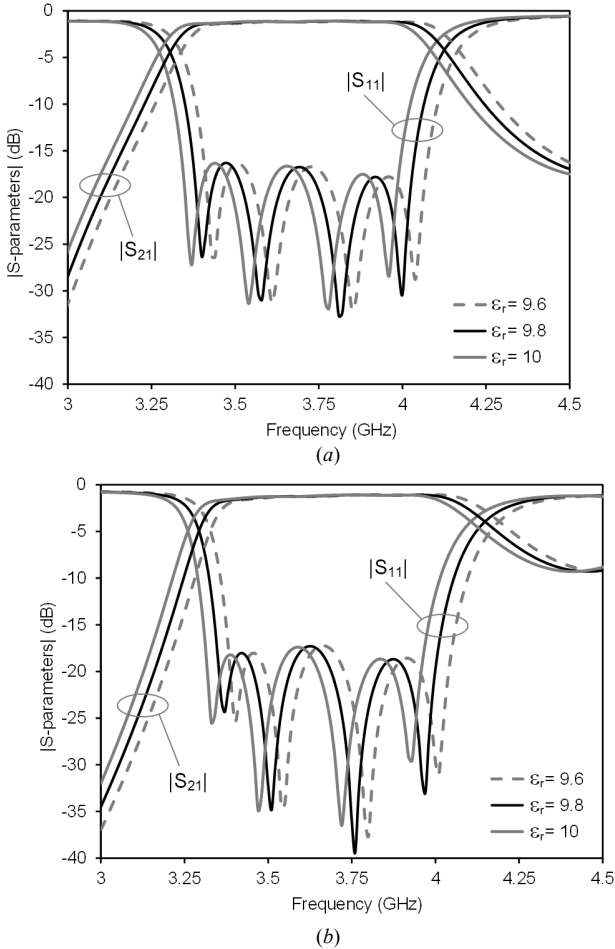

Fig. 9. Sensitivity analysis of the iris-type SIW filter and the perforated SIW filter with respect to the substrate dielectric permittivity (ε_r=9.8±0.2): (a) Spread of the scattering parameters of the iris-type SIW filter; (b) Spread of the scattering parameters of the perforated SIW filter (HFSS simulation).

the position of the perforated areas was changed with a maximum displacement of 50 μm; the relative position of the holes in each area was not modified, as the global shift represents the major effect in case of manufacturing by punching [25]. The two filters were compared in Fig. 8, which shows that the spread of the scattering parameters in the passband is more limited in the case of the perforated filter.

The deviation in the substrate dielectric permittivity is another potential source of error, able to jeopardize the filter performance. To investigate this effect and compare the perforated SIW filter and a classical iris-type SIW filter, the frequency response of the two structures was simulated in the case of nominal dielectric permittivity (ε_r=9.8) and in the cases of a deviation of ±0.2. Fig. 9 shows that in both structures the deviation in the dielectric permittivity determines a frequency shift, with no degradation of the bandwidth and the input matching level. More specifically, the frequency shift resulted ±35 MHz both in the case of the perforated SIW filter (Fig. 9(a)) and in the case of the iris-type SIW filter (Fig. 9(b)).
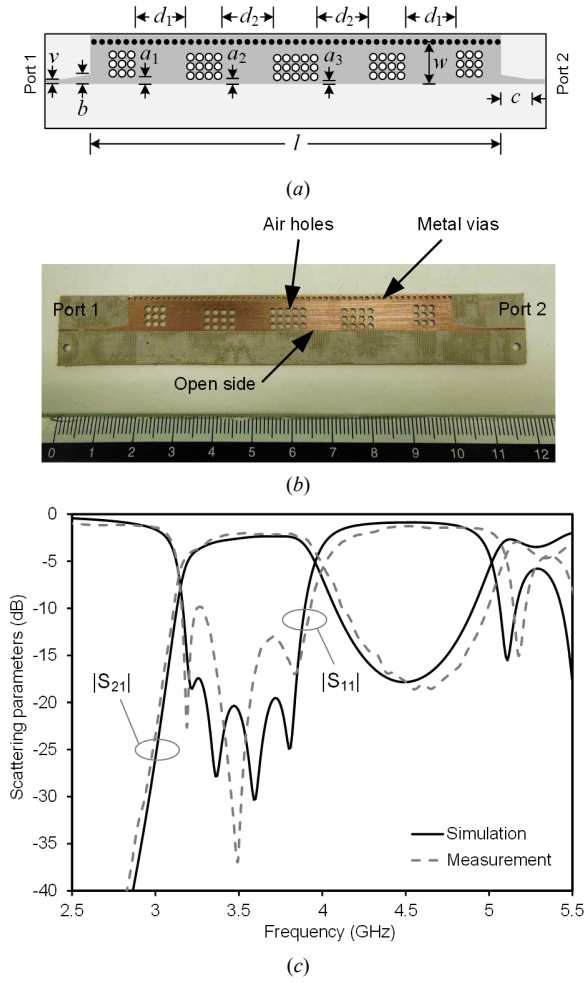
(a)

(b)

(c)

Fig. 10. Prototype of the four-pole filter based on perforated half-mode SIW structure: (a) Geometry of the filter (dimensions in mm: v=0.6, b=1.6, d_1=9.6, d_2=8.35, a_1=1, a_2=0.2, a_3=0.4, w=8.3, c=7, and l=83); (b) Photograph of the prototype; (c) Scattering parameters of the four-pole filter (HFSS simulation compared with measured data).

leakage. This reduction in the quality factor is more significant for the first and second mode, and it is marginal for the other two modes. For instance, in the fourth mode, the alternate phase of the electric field along the open boundary leads to very limited radiation. The variation of the modal quality factors determines the slope of the insertion loss of the filter.

TABLE II
RESONANCE FREQUENCY AND QUALITY FACTOR OF THE
FIRST MODES OF THE PERFORATED HALF-MODE SIW CAVITY

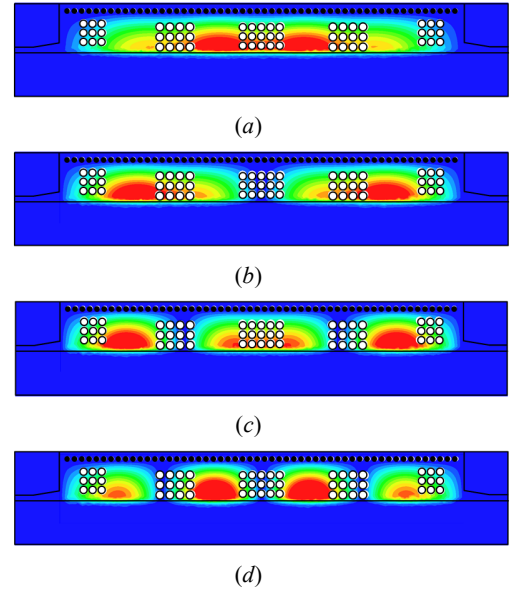| | Conductor and dielectric losses | | Conductor, dielectric and radiation losses | |
	Frequency (GHz)	Quality Factor	Frequency (GHz)	Quality Factor
Mode 1	3.30	187	3.19	61
Mode 2	3.44	186	3.28	103
Mode 3	3.70	185	3.55	146
Mode 4	4.00	198	3.90	184

Fig. 11. Amplitude of the electric modal field of the first resonant modes of the perforated half-mode SIW cavity: (a) First mode; (b) Second mode; (c) Third mode; (d) Fourth mode.

V. FOLDED FILTER BASED ON PERFORATED HALF-MODE SIW

A folded filter configuration was adopted to mitigate radiation losses of the half-mode SIW filter (Fig. 12(a)). By using this configuration, the open boundaries of the SIW structure are located face-to-face: this allows to reduce the radiation loss, especially for the first cavity mode, where the field exhibits a uniform phase along the entire open boundary. Moreover, the folded configuration introduces a direct input-output coupling, which determines transmission zero in the frequency response.

A three-pole half-mode SIW filter in folded configuration was designed by using HFSS. The design is aimed to locate the transmission zero close to the pass band. The geometry of the filter and the final dimensions are shown in Fig. 12(a). A prototype has been fabricated by milling machining, and a picture of the filter is shown in Fig. 12(b).

The comparison of simulated and measured scattering parameters is reported in Fig. 12(c), in the frequency band from 2.0 GHz to 7.0 GHz. The filter bandwidth, defined at 10 dB input matching, is 735 MHz in the simulation and 800 MHz in the measurement. The frequency of the transmission zero is 4.65 GHz in the simulation and 4.59 GHz in the measurement. The insertion loss at the central frequency f_0=3.65 GHz is 1.25 dB in the simulation and 1.20 dB in the measurement. Also in this case, the different contribution of losses have been investigated through simulations. Each transition contributes with a loss of 0.40 dB, whereas the SIW filter loss is 0.45 dB, which is attributed to dielectric loss (0.28 dB), and conductor loss (0.17 dB), and the contribution of radiation loss is negligible (0 dB). The primary effect of the

absence of radiation leakage is the flat insertion loss, as shown in Fig. 12c. The size of the circuit is practically identical to the half-mode SIW filter in Fig. 10, being the footprint area $(l+d_3+d_4)\times(2w+g)=693$ mm^2.

A different three-pole half-mode SIW filter in folded configuration was designed, to demonstrate that the frequency of the transmission zero can be easily controlled by changing the gap g (Fig. 12(a)). In this second design, the transmission zero was located at a higher frequency, with the aim to broaden the out-of-band rejection of the filter. The geometry of the filter is shown in Fig. 12(a), and the final dimensions are given in the caption of Fig. 13. A prototype has been fabricated by milling machining, and a picture of the filter is shown in Fig. 13(a).
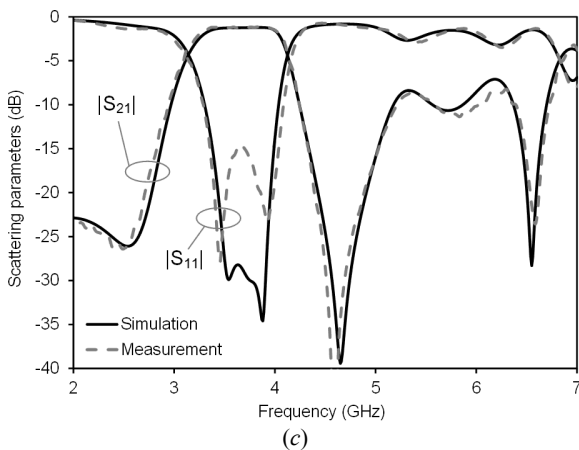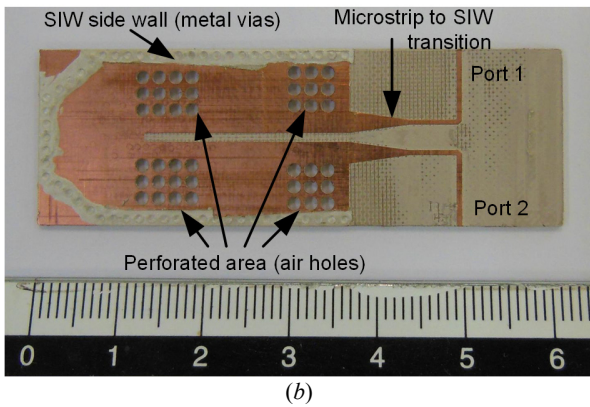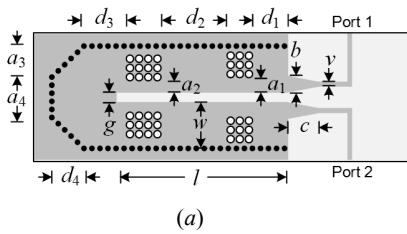
The comparison of simulated and measured scattering parameters is reported in Fig. 13(b), in the frequency band from 2.0 GHz to 7.0 GHz. The filter bandwidth, defined at 10 dB input matching, is 718 MHz in the simulation and 795 MHz in the measurement. A broad out-of-band rejection is found in the frequency response, with the transmission below -20 dB from 4.54 GHz to 6.02 GHz in the simulation, and from 4.54 GHz to 6.13 GHz in the measurement. The insertion loss at the central frequency $f_0=3.65$ GHz is 1.33 dB in the simulation and 1.68 dB in the measurement. Also in this case, the different contribution of losses have been investigated through simulations. Each transition contributes with a loss of 0.40 dB, whereas the SIW filter loss is 0.53 dB, which is attributed to dielectric loss (0.30 dB), conductor loss (0.19 dB), and very small radiation loss (0.04 dB). The size of the circuit is slightly larger than the one of the filter in Fig. 12, being the footprint area $(l+d_3+d_4)\times(2w+g)=728$ mm^2. It is worth noting that, while this filter does not exhibit outstanding out-of-band performance, the proposed filter geometry allows to improve the out-of-band rejection while keeping small size and easy fabrication.

Fig. 12. Prototype of the first three-pole folded filter based on perforated half-mode SIW structure: (a) Geometry of the filter (dimensions in mm: $v=0.6$, $b=2.6$, $d_1=1.65$, $d_2=10.56$, $d_3=3.9$, $d_4=6.7$, $a_1=2.45$, $a_2=1.95$, $a_3=5$, $a_4=9.45$, $w=9.2$, $c=7$, $g=1$, $l=25.1$); (b) Photograph of the prototype; (c) Scattering parameters of the three-pole filter (HFSS simulation compared with measured data).

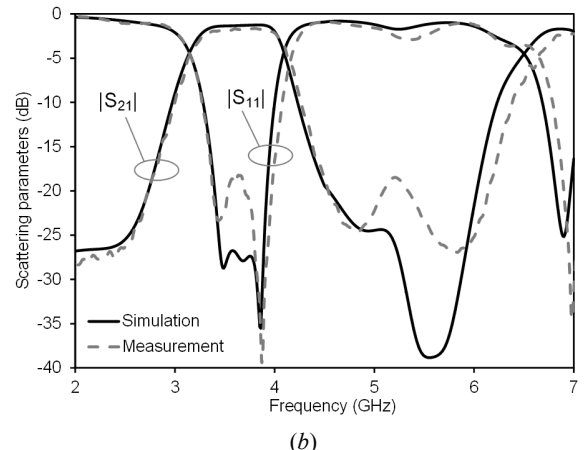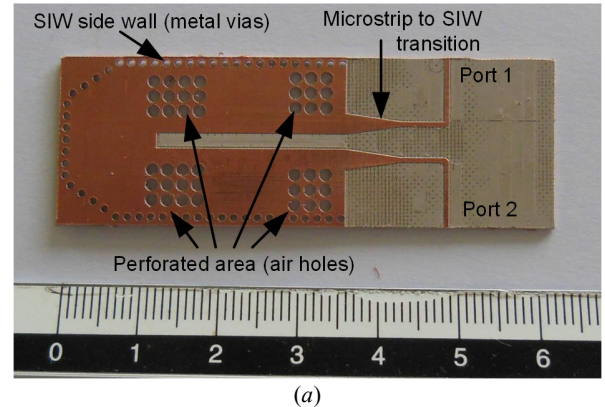Fig. 13. Prototype of the second three-pole folded filter based on perforated half-mode SIW structure (dimensions in mm: $v=0.6$, $b=2.6$, $d_1=1.65$, $d_2=10.56$, $d_3=3.9$, $d_4=6.7$, $a_1=2.45$, $a_2=1.95$, $a_3=5$, $a_4=9.45$, $w=9.2$, $c=7$, $g=2$, $l=25.1$): (a) Photograph of the prototype; (b) Scattering parameters of the three-pole filter (HFSS simulation compared with measured data).

VI. Conclusion

A new class of substrate integrated waveguide filters has been proposed in this paper. The use of periodic perforations in the dielectric substrate allows to introduce evanescent waveguide sections, which behave as immitance inverters. This solution leads to the design of compact resonators and filters with low sensitivity to fabrication inaccuracies.

Analytical formulas for the design of the immitance inverters have been derived, which represent a useful tool for the direct synthesis of filters. The use of full-wave simulations for the fine tuning of the inverter geometry has been also discussed.

Four SIW filters have been designed and experimentally validated. They allow to demonstrate the feasibility of the proposed structures and the usefulness of the design formulas, the filter performance in comparison with iris-type filters, the effect of radiation loss in the case of half-mode SIW structures and the technique to mitigate this loss, and the possibility to introduce and control transmission zeros.

Appendix

The ABCD matrix of an impedance inverter is

$$\begin{bmatrix} A & B \\ C & D \end{bmatrix} = \begin{bmatrix} 0 & jK \\ j/K & 0 \end{bmatrix} \tag{15}$$

and the corresponding scattering matrix is

$$[S] = \frac{1}{K^2 + Z_1 Z_2} \begin{bmatrix} K^2 - Z_1 Z_2 & j2K\sqrt{Z_1 Z_2} \\ j2K\sqrt{Z_1 Z_2} & K^2 - Z_1 Z_2 \end{bmatrix} \tag{16}$$

being Z_1 and Z_2 the reference impedance of port 1 and 2, respectively. In the particular case of $Z_1 = Z_2 = Z_0$

$$[S] = \frac{1}{K^2 + Z_0^2} \begin{bmatrix} K^2 - Z_0^2 & j2KZ_0 \\ j2KZ_0 & K^2 - Z_0^2 \end{bmatrix} \tag{17}$$

when Z_0 is real, $S_{11} = S_{22}$ is real while $S_{21} = S_{12}$ is imaginary. Considering that this is a scattering matrix of a lossless component, S_{22} is completely determined by S_{11} (apart for the sign). This means that each component having S_{11} real is an impedance inverter and its value can be evaluated as

$$K = \sqrt{Z_1 Z_2} \sqrt{\frac{1 + S_{11}}{1 - S_{11}}} \tag{18}$$

References

[1] R. Garg, I. Bahl, and M. Bozzi, *Microstrip Lines and Slotlines*, Third Edition, Artech House, 2013.

[2] M. Bozzi, A. Georgiadis, K. Wu, "Review of Substrate Integrated Waveguide (SIW) Circuits and Antennas," *IET Microwaves Antennas Propag.*, vol. 5, no. 8, pp. 909-920, June 2011.

[3] N. Grigoropoulos, B.S. Izquierdo, and P.R. Young, "Substrate Integrated Folded Waveguides (SIFW) and Filters," *IEEE Microw. Compon. Lett.*, vol. 15, no. 12, pp. 829-831, Dec. 2005.

[4] W. Che, L. Geng, K. Deng, and Y. L. Chow, "Analysis and Experiments of Compact Folded Substrate-Integrated Waveguide," *IEEE Trans. Microw. Theory Techn.*, vol. 56, no. 1, pp. 88-93, Jan. 2008.

[5] W. Hong *et al.*, "Half Mode Substrate Integrated Waveguide: A New Guided Wave Structure for Microwave and Millimeter Wave Application," *Proc. Joint 31st International Conference on Infrared Millimeter Waves and 14th International Conference on Terahertz Electronics*, p. 219, Shanghai, China, Sept. 18–22, 2006.

[6] Q. Lai, C. Fumeaux, W. Hong, and R. Vahldieck, "Characterization of the Propagation Properties of the Half-Mode Substrate Integrated Waveguide," *IEEE Trans. Microw. Theory Techn.*, Vol. 57, No. 8, pp. 1996-2004, Aug. 2009.

[7] M. Bozzi, D. Deslandes, P. Arcioni, L. Perregrini, K. Wu, and G. Conciauro, "Efficient Analysis and Experimental Verification of Substrate Integrated Slab Waveguides for Wideband Microwave Applications," *International Journal of RF and Microwave Computer–Aided Engineering*, vol. 15, no. 3, pp. 296-306, May 2005.

[8] M. Bozzi, S. A. Winkler, and K. Wu, "Broadband and compact ridge substrate-integrated waveguides," *IET Microwaves, Antennas and Propagation*, vol. 4, no. 11, pp. 1965–1973, Nov. 2010.

[9] S. Moscato, R. Moro, M. Pasian, M. Bozzi, and L. Perregrini, "Two-Material Ridge Substrate Integrated Waveguide for Ultra-Wide Band Applications," *IEEE Trans. Microw. Theory Techn.*, vol. 63, no. 10, pp. 3175-3182, Oct. 2015.

[10] F. Parment, A. Ghiotto, T. P. Vuong, J. M. Duchamp, and K. Wu, "Air-Filled Substrate Integrated Waveguide for Low-Loss and High Power-Handling Millimeter-Wave Substrate Integrated Circuits," *IEEE Trans. Microw. Theory Techn.*, vol. 63, no. 4, pp. 1228-1238, April 2015.

[11] X.-P. Chen and K. Wu, "Substrate Integrated Waveguide Filter: Basic Design Rules and Fundamental Structure Features," *IEEE Microw. Mag.*, vol. 15, no. 5, pp. 108-116, July-Aug. 2014.

[12] X.-P. Chen and K. Wu, "Substrate Integrated Waveguide Filters: Design Techniques and Structure Innovations," *IEEE Microwave Magazine*, vol. 15, no. 6, pp. 121-133, Sept.-Oct. 2014.

[13] X.-P. Chen and K. Wu, "Substrate Integrated Waveguide Filters: Practical Aspects and Design Considerations," *IEEE Microw. Mag.*, vol. 15, no. 7, pp. 75-83, Nov.-Dec. 2014.

[14] R. Moro, S. Moscato, M. Bozzi, and L. Perregrini, "Substrate Integrated Folded Waveguide Filter with Out-of-Band Rejection Controlled by Resonant-Mode Suppression," *IEEE Microw. Compon. Lett.*, vol. 25, no. 4, pp. 214-216, April 2015.

[15] Q. L. Zhang, B. Z. Wang, D. S. Zhao, and K. Wu, "A Compact Half-Mode Substrate Integrated Waveguide Bandpass Filter With Wide Out-of-Band Rejection," *IEEE Microw. Compon. Lett.*, vol. 26, no. 7, pp. 501-503, July 2016.

[16] S. Moscato, C. Tomassoni, M. Bozzi, and L. Perregrini, "Quarter-Mode Cavity Filters in Substrate Integrated Waveguide Technology," *IEEE Trans. Microw. Theory Techn.*, vol. 64, no. 8, pp. 2538-2547, Aug. 2016.

[17] P. Chu *et al.*, "Wide Stopband Bandpass Filter Implemented With Spur Stepped Impedance Resonator and Substrate Integrated Coaxial Line Technology," *IEEE Microw. Compon. Lett.*, vol. 24, no. 4, pp. 218-220, April 2014.

[18] M. Salehi and E. Mehrshahi, "Spurious-Response Suppression of Substrate Integrated Waveguide Filters Using Multishape Resonators and Slotted Plane Structures," *Int. J. RF and Microwave Comp. Aid Eng.*, vol. 21, no. 6, pp. 650–657, Nov. 2011.

[19] M. Salehi, J. Bornemann, and E. Mehrshahi, "Substrate-Integrated Waveguide Band Pass Filters with Frequency-Dependent Coupling Elements," *Int. J. RF and Microwave Comp. Aid Eng.*, vol. 24, no. 2, pp. 237–242, Mar. 2014.

[20] A. Pourghorban Saghati, A. Pourghorban Saghati, and K. Entesari, "Ultra-Miniature SIW Cavity Resonators and Filters," *IEEE Trans. Microw. Theory Techn.*, vol. 63, no. 12, pp. 4329-4340, Dec. 2015.

[21] J. Schorer, J. Bornemann, and U. Rosenberg, "Mode-Matching Design of Substrate Mounted Waveguide (SMW) Components," *IEEE Trans. Microw. Theory Techn.*, vol. 64, no. 8, pp. 2401-2408, Aug. 2016.

[22] A. Coves *et al.*, "A Novel Band-Pass Filter Based on a Periodically Drilled SIW Structure," *Radio Science*, vol. 51, no. 4, pp. 328–336, April 2016.

[23] L. Silvestri, E. Massoni, C. Tomassoni, A. Coves, M. Bozzi, and L. Perregrini, "Modeling and Implementation of Perforated SIW Filters," *IEEE MTT-S Int. Conf. Numerical Electromagnetic and Multiphysics Modeling and Optimization* (NEMO2016), Beijing, China, July 27-29, 2016.

[24] L. Silvestri, E. Massoni, C. Tomassoni, A. Coves, M. Bozzi, and L. Perregrini, "A New Class of SIW Filters Based on Periodically Perforated Dielectric Substrate," *46th European Microwave Conf.* (EuMC2016), London, UK, Oct. 3–7, 2016.

[25] M. Pasian, M. Bozzi, and L. Perregrini, "Low-cost Dichroic Mirrors Manufactured by Punching Technique," *Intern. Journal of Microwave and Wireless Technologies*, vol. 3, no. 6, pp. 595–600, Dec. 2011.

[26] Y. Cassivi, L. Perregrini, P. Arcioni, M. Bressan, K. Wu, and G. Conciauro, "Dispersion Characteristics of Substrate Integrated Rectangular Waveguide," *IEEE Microw. Compon. Lett.*, vol. 12, no. 9, pp. 333-335, Sept. 2002.

Lorenzo Silvestri was born in Novara, Italy, in 1987. He received the Master degree in Electronic Engineering in 2014 at the University of Pavia. He is currently working as a post-graduate scholar at the Department of Industrial and Information Technology (University of Pavia). His main interest are related to the development of new components in substrate integrated waveguide (SIW) technology on innovative substrate materials.
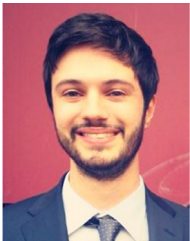
Enrico Massoni (S'14) was born in Broni, Italy, in 1991. He received the B.S. degree in Electronics and Telecommunications and the M.S. degree in Electronic Engineering from the University of Pavia, Pavia, Italy, in 2013 and 2015, respectively. He is currently working towards his Ph.D. degree within the Microwave Laboratory group of the Electrical, Computer and Biomedical Engineering Dept. at the University of Pavia. His research activities mainly deal with the design and implementation of new passive interconnects and components, mostly in substrate-integrated waveguide and non-radiative technology, via additive manufacturing techniques of novel 3D-printed materials for RF and microwaves systems.

He received the first prize at the "Graduate Student Challenge" at IMS2014 in Tampa, FL, the first prize at the "Student Challenge" at the 46th European Microwave Conference in London, UK, in 2016, and the "Best Poster Award" at the IEEE Circuit and Systems Society CAS-day event in Como, Italy, in 2016.

He has been the Chair of the IEEE Student Branch of Pavia (recipient of the 2016 "Exemplary Student Branch Award" – Italy Section – R8) and the Founder and Chair of the MTT-S Student Branch Chapter of Pavia.

Cristiano Tomassoni (M'15) was born in Spoleto, Italy. He received the Laurea degree and Ph.D. degree in electronics engineering from the University of Perugia, Perugia, Italy, in 1996 and 1999, respectively. His dissertation concerned the mode-matching analysis of discontinuities involving elliptical waveguides.

In 1999, he was a Visiting Scientist with the Lehrstuhl für Hochfrequenztechnik, Technical University of Munich, Munich, Germany, where he was involved with the modeling of waveguide structures and devices by using the generalized scattering matrix (GSM) technique. From 2000–2007, he was a Postdoctoral Research Associate with the University of Perugia. In 2001, he was a Guest Professor with the Fakultät für Elektrotechnik und Informationstechnik, Otto-von-Guericke University, Magdeburg, Germany. During that time, he was involved with the modeling of horn antennas having nonseparable cross sections by using hybrid methods combining three different techniques: the finite-element method, mode-matching technique, and generalized multipole technique. He was also involved in the modeling of low-temperature co-fired ceramics by using the method of moments. He studied new analytical methods to implement boundary conditions in the transmission-line matrix method, and he modeled aperture antennas covered by dielectric radome by using spherical waves. Since 2007, he has been an Assistant Professor with the University of Perugia. His main area of research concerns the modeling and design of waveguide devices and antennas. His research interests also include the development of reduced-size cavity filters, reconfigurable filters, and printed reconfigurable antenna arrays. Dr. Tomassoni was the recipient of the 2012 Microwave Prize presented by the IEEE Microwave Theory and Technique Society.

Angela Coves received the Licenciado degree in physics and the Ph.D. degree in physics from the Universidad de Valencia, Valencia, Spain, in 1999 and 2004, respectively. She became a Lecturer with the Universidad Miguel Hernández Elche, in 2001. Her current research interests include the analysis and design of microwave passive components, periodic structures, and RF breakdown high power effects.

Maurizio Bozzi (S'98–M'01–SM'12) was born in Voghera, Italy, in 1971. He received the Ph.D. degree in electronics and computer science from the University of Pavia, Pavia, Italy, in 2000.

He held research positions with various universities worldwide, including the Technische Universität Darmstadt, Germany; the Universitat de Valencia, Spain; and the École Polytechnique de Montréal, Canada. In 2002, he joined the Department of Electronics, University of Pavia, where he is currently an Associate Professor of electromagnetic fields (with Full Professor habilitation). He is also a Guest Professor of the Tianjin University (China) for the term 2015-2017.

He has authored or co-authored more than 100 journal papers and 260 conference papers. He co-edited the book *Periodic Structures* (Research Signpost, 2006) and co-authored the book *Microstrip Lines and Slotlines* (Artech House, 2013). His main research interests concern the computational electromagnetics, the substrate integrated waveguide technology, and the use of novel materials and fabrication technologies for microwave circuits (including paper, textile, and 3D printing).

Prof. Bozzi is an Elected Member of the Administrative Committee of the IEEE Microwave Theory and Techniques Society (MTT-S) for term 2017–2019 and a Co-Chair of the Meeting and Symposia Committee of MTT-S AdCom for year 2017. He was the Secretary of IEEE MTT-S for year 2016 and a member of the General Assembly (GA) of the European Microwave Association (EuMA) for the term 2014–2016. He is an associate editor for the IEEE MICROWAVE AND WIRELESS COMPONENTS LETTERS, the IET Electronics Letters, and the IET Microwaves, Antennas and Propagation. He is the General Chair of the IEEE MTT-S International Microwave Workshop Series-Advanced Materials and Processes (IMWS-AMP 2017), Pavia, Italy, 2017. He was the General Chair of the IEEE International Conference on Numerical Electromagnetic Modeling and Optimization (NEMO2014), Pavia, Italy, 2014, and the General Chair of the IEEE MTT-S International Microwave Workshop Series on Millimeter Wave Integration Technologies, Sitges, Spain, 2011.

He received several awards, including the 2015 Premium Award for Best Paper in IET Microwaves, Antennas & Propagation, the 2014 Premium Award for the Best Paper in Electronics Letters, the Best Student Paper Award at the 2016 IEEE Topical Conference on Wireless Sensors and Sensor Networks (WiSNet2016), the Best Paper Award at the 15th Mediterranean Microwave Symposium (MMS2015), the Best Student Award at the 4th European Conference on Antennas and Propagation (EuCAP 2010), the Best Young Scientist Paper Award of the XXVII General Assembly of URSI in 2002, and the MECSA Prize of the Italian Conference on Electromagnetics (XIII RiNEm), in 2000.

Luca Perregrini (M'97-SM'12-F'16) was born in Sondrio, Italy, in 1964. He received the "Laurea" degree in Electronic Engineering and the Ph.D. in Electronics and Computer Science in 1989 and 1993, respectively. In 1992 he joined the Faculty of Engineering of the University of Pavia, he is now full professor of electromagnetic fields and responsible of the Microwave Laboratory. He has been the tutor of several Ph.D. students and the supervisor of many MS and BS students. He has been a visiting professor at the École Polytechnique de Montréal, Québec, Canada in 2001, 2002, 2005, and 2006.

Prof. Perregrini has been responsible of many research contracts with prominent international research centers and companies. His main research interests have been focused on the development of numerical methods for electromagnetics, and the design of microwave components and antennas.

He is Fellow of the Institute of Electrical and Electronics Engineers (IEEE), a member of the Technical Committee MTT–15 (Microwave Field Theory) of IEEE MTT Society, member of the Board of Directors of the European Microwave Association (EuMA), member of the Società Italiana di Elettromagnetismo (SIEm), and he has been a member of the General Assembly of EuMA (2011-2013).

Prof. Perregrini is currently Editor in Chief of the IEEE TRANSACTIONS ON MICROWAVE THEORY AND TECHNIQUE. He also serves as Associate Editor of the International Journal of Microwave and Wireless Technologies (since 2011), IET Electronic Letters (since 2015), and of the International Journal of Microwave and Wireless Technologies (June 2015). He was Associate Editor of the IEEE MICROWAVE AND WIRELESS COMPONENTS LETTERS (2010-2013) and of IEEE TRANSACTIONS ON MICROWAVE THEORY AND TECHNIQUES (2013-2016)), and Gest Editor of the IEEE TRANSACTIONS ON MICROWAVE THEORY AND TECHNIQUES (Jan. 2015). He co-edited the book Periodic Structures, (Research Signpost, 2006). He is the appointed General Conference Chair of the European Microwave Week 2020 (Rome, Italy), the Technical Program Committee Chair of the International Microwave Workshop Series on Advanced Materials and Processes (IMWS-AMP 2017) (Pavia, Italy, Sept. 2017), and he was the Technical Program Committee Chair of the IEEE MTT-S International Conference on Numerical Electromagnetic Modeling and Optimization (NEMO2014) (Pavia, Italy, May 2014), and of the European Microwave Conference (Rome, Italy, Oct. 2014). He also served as a member of prize committees for several conferences/societies.

Prof. Perregrini has been an invited speaker at many conferences, and has delivered invited seminar talks in Universities and research centers worldwide. He was the co-recipient of the Best Paper Award at the 15th Mediterranean Microwave Symposium (MMS2015), of the Best Student Paper Award at the 4th European Conference on Antennas and Propagation (EuCAP 2010), and the 2nd Best Student Paper Award at the 27th Int. Review of Progress in Applied Computational Electromagnetics (ACES 2010). He authored or co-authored more than 80 journal papers and more than 230 conference papers, 6 book chapters, and 2 textbooks.